Results in Physics 68 (2025) 108073

Contents lists available at ScienceDirect

Results in Physics

journal homepage: www.elsevier.com/locate/rinp

Electrocatalytic detection of Acetaminophen by sodium ferrite

Saima Perveen [a,b], Jameel Ahmed Baig [a,*], Mohammad Nur-e-Alam [c], Mohsin Kazi [d], Shahabuddin Memon [a], Tasneem Gul Kazi [a], Khalil Akhtar [a], Sajjad Hussain [e]

[a] Centre of Excellence in Analytical Chemistry, University of Sindh, Jamshoro 76080, Pakistan
[b] Pamukkale University, Faculty of Science, Chemistry Department, Pamukkale, Denizli, Turkey
[c] Department of Pharmacognosy, College of Pharmacy, King Saud University, PO Box, 2457, Riyadh 11451, Saudi Arabia
[d] Department of Pharmaceutics, College of Pharmacy, King Saud University, PO Box, 2457, Riyadh 11451, Saudi Arabia
[e] Centre of Excellence in Solid State Physics, University of the Punjab, Lahore, 05422, Pakistan

ARTICLE INFO

Keywords:
Electrochemical analysis, sodium ferrite nanoparticles
Differential pulse voltammetry
Glassy carbon electrode
Acetaminophen

ABSTRACT

Acetaminophen (APN) is a safer alternative to opioids and is recognized for its analgesic and antipyretic properties. Prolonged usage and overdose of APN cause severe health problems for humans. Hence, its monitoring in the human body, pharmaceutical preparations and consumption sources is important. Thus, the current study was designed to synthesize the sodium ferrite nanoparticles ($Na_2Fe_4O_7$-NPs) based on the *Tamarindus indica* fruit extract for selective trace electrochemical detection of APN. The $Na_2Fe_4O_7$-NPs were characterized by advanced analytical techniques such as x-ray diffraction (XRD), fourier transform infrared (FTIR), UV–visible, atomic force microscopy (AFM), zeta potential, zeta sizer, energy dispersive x-ray (EDX) and field emission scanning electron microscopy (FESEM) which displayed that the $Na_2Fe_4O_7$-NPs possess hexagonal structure, a narrow band gap (1.475 eV), corresponding to their excellent electronic capability, nanosize of particles, rough surface and highly stable nature for electrochemical analysis. $Na_2Fe_4O_7$-NPs were deposited on a glassy carbon electrode (GCE) to manufacture an electrochemical sensor ($Na_2Fe_4O_7$-NPs/GCE) and characterized its surface behaviour by cyclic voltammetry. $Na_2Fe_4O_7$-NPs/GCE voltammetric sensor showed its selective sensing of APN in a wide dynamic range (1.0×10^{-8} to 4.5×10^{-4} M) with a detection limit of 2.72 10^{-9} M. Further, the developed method showed excellent stability in addition to reproducibility for the sensing of APN (% RSD < 5.0). The developed electrochemical sensor was found to be efficient for selective and sensitive detection of APN in real samples with quantitative recoveries (> 90 %).

Background

Acetaminophen (APN; paracetamol, N-acetyl-p-aminophenol, or 4-acetaminophen) is famous as a safer alternative to opioids due to its pain-relieving properties. It is an extensively used pharmaceutical for actively dealing with cancer pain, fever, and headache [1]. APN exhibits active therapeutic effects with insignificant opposing reactions at recommended levels [2]. However, excessive dosage of drugs can lead to liver damage, nausea, renal failure, stomach pain, and vomiting [3,4]. Moreover, inappropriate discarding of in-use drugs through drainage systems pollutes the environment and affects life [5]. Thus, there is a need to develop precise techniques for the accurate monitoring of APN in biological and environmental matrices. Various methodologies such as capillary electrophoresis [6], high-performance liquid chromatography [7,8], and spectrophotometry [9] were reported for the detection of APN. Despite the high accuracy, these analytical methods have disadvantages as the equipment is expensive and consumes more time in detection. Therefore, establishing an accessible, accurate, fast, cost-effective, and susceptible analytical method is important for assessing the concentration of APN.

An electrochemical method is a promising alternative and offers high sensitivity, simple sample pre-treatment, eco-friendly, fast response, good selectivity, and accuracy with excellent environmental compatibility [10]. These are important in the quantification of numerous analytes in biological, environmental, and pharmaceutical samples by detecting electrical signals produced from the interaction (oxidation or reduction) between the analytes and the electrode surface [11]. For determining the concentration of APN, it is crucial to create an analytical method that is simple to use, precise, rapid, cost-effective, and highly sensitive [12,13].

* Corresponding author.
E-mail address: jameel.baig@usindh.edu.pk (J.A. Baig).

https://doi.org/10.1016/j.rinp.2024.108073
Received 1 October 2024; Received in revised form 2 December 2024; Accepted 5 December 2024
Available online 9 December 2024

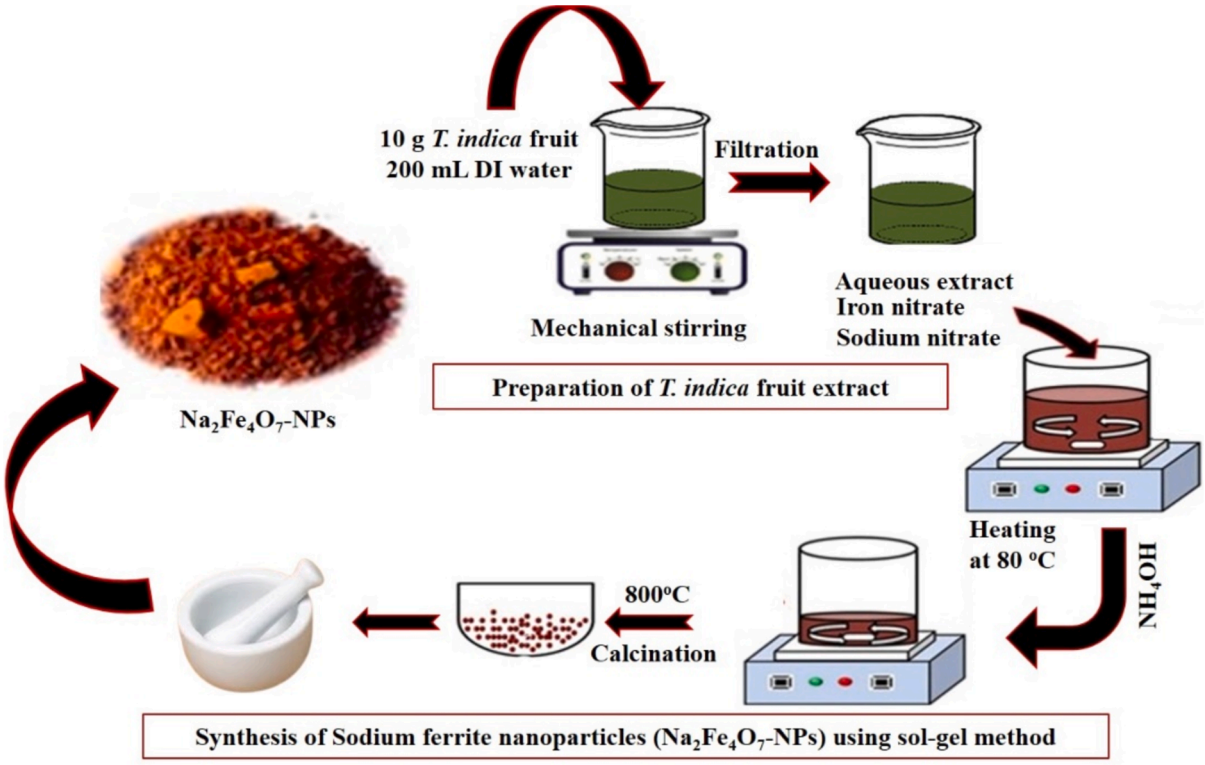

Fig. 1. Schematic diagram of synthesis of $Na_2Fe_4O_7$-NPs by sol–gel method.

Chemical modification of electrochemical sensors is required to increase their structural, electrocatalytic, surface, and charge carrier mobilization properties [14]. Currently, various functional nanomaterials, such as magnetite-coated reduced graphene oxide (Fe_3O_4-rGO) nanocomposites [4], silver nanoparticles (AgNPs) [15], spinel vanadium nanoferrites (VFe_2O_4) [16], spinel magnesium sodium ferrite ($Mg_{1-x}Na_xFe_2O_4$) [17], yttrium doped cobalt spinel ferrite ($CoY_xFe_{2-x}O_4$) [18], and Perovskite Bismuth ferrite ($BiFeO_3$) [19] and perovskite lanthanum ferrites ($LaFeO_3$) [20] are performing vital roles in improving the activity of electrochemical sensors [21].

In recent studies, nanoferrites are attractive materials for sensor materials in many industries [22,23]. Generally, ferrites are ceramic materials of iron oxide and other metallic elements, such as nickel, zinc, and manganese [24]. They exhibit excellent magnetic properties, including high magnetization, low coercivity, and good chemical stability [25,26]. Ferrites are inexpensive and have low toxicity, making them ideal for various industrial applications [27]. These materials are worthwhile in various sensor applications due to their physiological features, simple surface functionalization, and high surface area-to-volume ratio [28].

Traditionally, nanosized particles can be synthesized by biological, chemical, and physical methods. Among them, chemical and physical methods frequently contain unsafe chemicals, resulting in numerous biological hazards, and are expensive. However, the biological method shows more effectiveness, low toxicity, and eco-friendly nature as compared to other methods [29,30]. The biological methods are based on living organisms such as plants and microorganisms. Various parts of plants are used for the synthesis. It is because their extract may have organic (amino acids, ascorbic acid, gluconic acid, glucose, starch) and inorganic compounds that may act as stabilizing agents or capping agents to overcome aggregations [31]. Among various green synthesis methods, the sol–gel auto combustion method is superior as it is easy to handle, has high purity, controlled size distribution, precise chemical stoichiometry, and has the most negligible impact on electrical and magnetic properties [32].

The hexagonal ferrites are preferable over spinel and perovskite ferrites due to their unique structural and electrochemical advantages [33–35]. The hexagonal structure of these ferrites offers a stable crystallographic structure with enhanced adsorption sites that facilitate strong interactions with drug molecules for their sensitive and accurate electrochemical detection [33]. Additionally, these ferrites have high surface area and favourable morphology supporting efficient electron transfer, enhancing signal response, particularly for drugs like APN [33]. In contrast, spinel and perovskite ferrites, which generally possess cubic or orthorhombic structures, lack these specific interaction sites and may not provide the same level of sensitivity required for precise drug-target applications [36–38]. Therefore, the current work was designed to employ green technology for the synthesis of $Na_2Fe_4O_7$-NPs using *Tamarindus indica* (*T. indica*) fruit extract. The $Na_2Fe_4O_7$-NPs were utilized to fabricate $Na_2Fe_4O_7$-NPs based modified glassy carbon electrode ($Na_2Fe_4O_7$/GCE) for quantitative electrochemical detection of APN. The synthesized $Na_2Fe_4O_7$-NPs were characterized by advanced analytical techniques. To ensure consistent effectiveness, experimental parameters such as scan rate, pH, electrolyte, and voltammetric mode were optimized. The efficacy of the sensor to detect APN in biological, pharmaceutical, and wastewater samples was validated by measurement of its accuracy, precision, and repeatability.

Methods

Chemicals and reagents

Analytical-grade reagents were employed in the current study. Acetaminophen (≥99%), glucose ($C_6H_{12}O_6$), amoxicillin ($C_{16}H_{19}N_3O_5S$), potassium chloride (KCl), uric acid ($C_5H_4N_4O_3$), sodium acetate (CH_3COONa), ascorbic acid ($C_6H_8O_6$), hydroquinone ($C_6H_6O_2$), levofloxacin ($C_{18}H_{20}FN_3O_4$), nafion ($C_7HF_{13}O_5S{\cdot}C_2F_4$), nitric acid ($HNO_3$), phosphorous acid ($H_3PO_3$), sodium nitrate ($NaNO_3$), sodium phosphate dibasic (Na_2HPO_4), phosphoric acid (H_3PO_4), sodium phosphate monobasic (NaH_2PO_4), Iron (III) nitrate nonahydrate or Fe

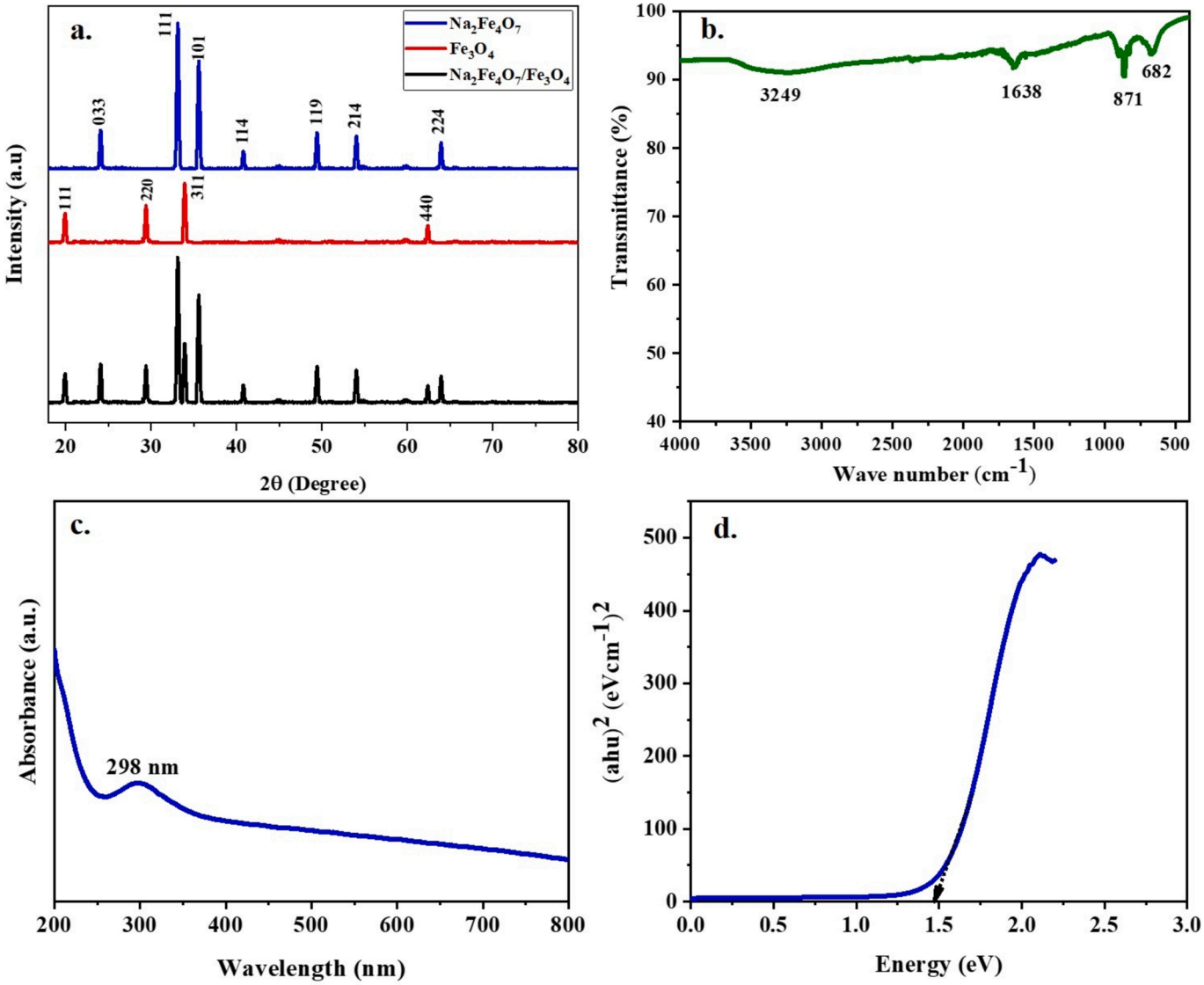

Fig. 2. **a.** XRD spectrum **b.** FTIR spectrum **c.** UV–visible spectrum and **d.** Tauc plot of synthesized $Na_2Fe_4O_7$-NPs.

$(NO_3)_3{\cdot}9H_2O$, sucrose ($C_{12}H_{22}O_{11}$), ethanol (C_2H_5OH), ferricyanide; $[Fe(CN)_6]^{3-}$ and acetic acid (CH_3COOH), were purchased from Sigma-Aldrich (Louis, USA).

Sol-gel synthesis of $Na_2Fe_4O_7$-NPs

The *Tamarindus indica* (*T. indica*) fruit was collected from the departmental garden of the university located at Jamshoro Sindh Pakistan. The whole fruit of *T. indica* was cleaned with deionized (DI) water and separated from the fruit pulp. The obtained pulp (10 g) was mixed in 200 mL DI water and heated with continuous stirring at 80 °C for 4h on the hot plate. The resulting solution was filtrated to separate the extract [39]. For the synthesis of $Na_2Fe_4O_7$-NPs, 100 mL solution of $Fe(NO_3)_3{\cdot}9H_2O$ (2.0 M) and sodium nitrate (1.0 M) were mixed with constant stirring at a neutral pH for 30 min. The *T. indica* extract was treated with the resulting solution of precursor salts followed by continuous heating at 80 °C to obtain the gel based on the sol–gel method. The gel was dried in an oven and ground. The obtained powder was calcined for 5h at 800 °C [40,41] (Fig. 1).

Fabrication of $Na_2Fe_4O_7$-NPs-based sensor

The glassy carbon electrode (GCE) was polished and sonicated in DI water. The sonicated GCE was washed separately with nitric acid (50%) and ethanol [42]. 5 mg of $Na_2Fe_4O_7$-NPs were mixed with 10 mL of DI water and 100 μL nafion in an ultrasonic water bath for 30 min. The prepared dispersion was dropped onto the surface of GCE by micropipette and dried overnight to obtain $Na_2Fe_4O_7$-NPs/GCE [43].

Characterization techniques

The XRD (D-8, Bruker, Germany) and Fourier transform infrared (FTIR) spectrometer (Madison, Wisconsin-based Thermo Electron Scientific) were employed to study the structure and functionalities of synthesized nanoparticles. The UV–visible spectrophotometer (Shimadzu, Kyoto, Japan) and atomic force microscopy (AFM; Nano-Scope V, Bruker, Germany) instruments were used to study the band gap and surface topography of $Na_2Fe_4O_7$-NPs respectively. The Zeta potential analyzer (ELSZ-2000) was employed to study the stability and zeta size of $Na_2Fe_4O_7$-NPs. The energy dispersive x-rays (EDX) and field emission scanning electron microscopy (FESEM) were accessed from Bruker (USA) to study the morphology and elemental composition of $Na_2Fe_4O_7$-

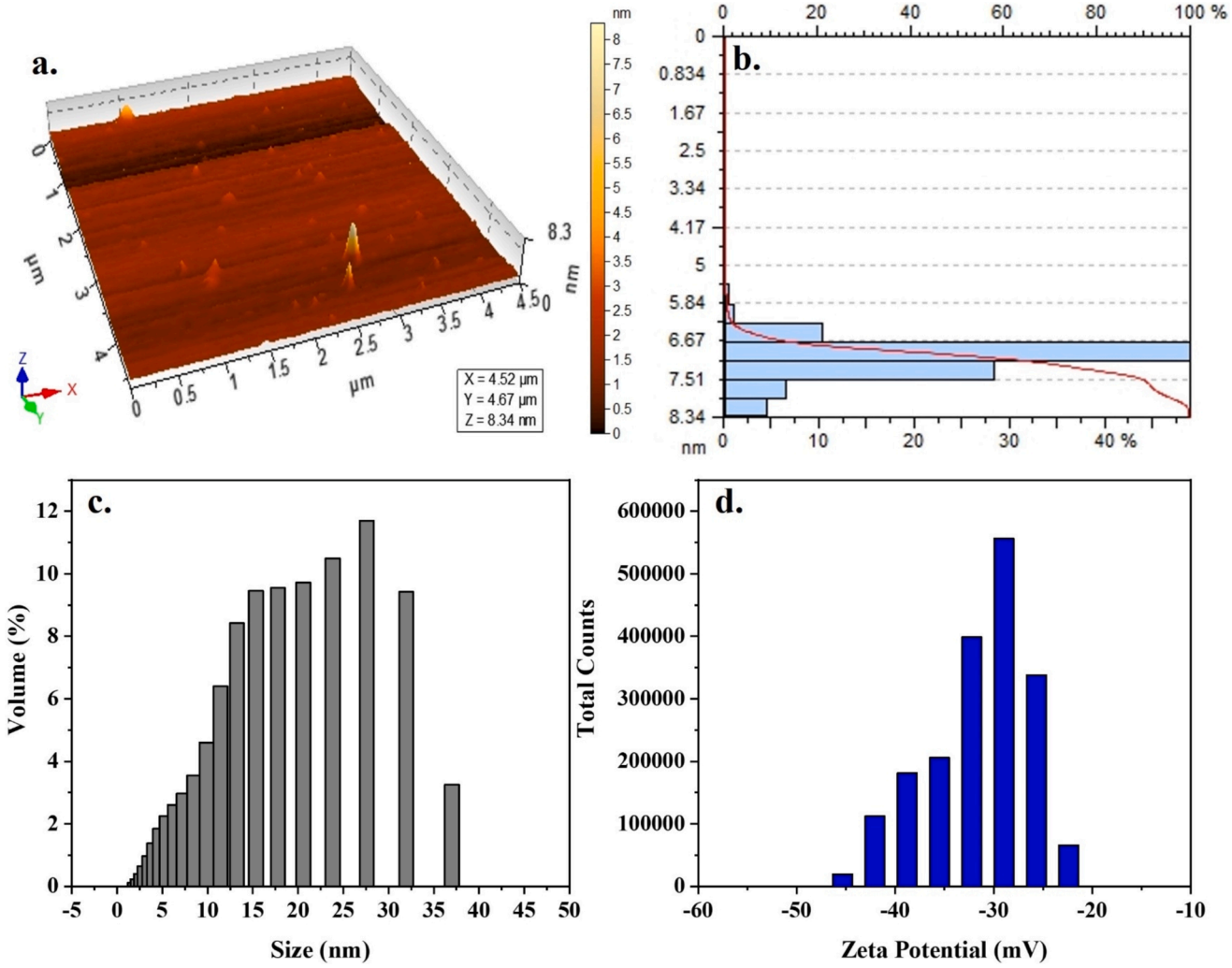

Fig. 3. **a.** AFM 3D Topography, **b.** AFM bar graph of size distribution, **c.** hydrodynamic size distribution, and **d.** zeta potential of $Na_2Fe_4O_7$-NPs.

NPs. The CHI electrochemical analyzer (Austin, USA) was used to detect APN.

Sampling, and sample preparation

The blood (n = 5), and urine (n = 5) samples were obtained from healthy volunteer human subjects, belonging to Hyderabad and Jamshoro cities. The wastewater samples (n = 5) were sampled from the effluent discharged sites of the pharmaceutical industry, district Jamshoro. All the samples were subjected to filtration to remove all the insoluble materials. The blood samples were further centrifuged to separate the serum. The pharmaceutical tablet samples (n = 9) were purchased from different national/multinational companies. The tablet samples were ground by pestle and mortar. The solution for each tablet was prepared by dissolving an appropriate amount in 10 mL of DI water in an ultrasonic water bath for 15 min. The resultant solutions of real samples were stored at 4.0 °C in the dark.

Voltammetric analysis

An electrochemical analyzer with a three-electrode (auxiliary electrode; platinum wire, reference electrode; silver/silver chloride, and working electrode; $Na_2Fe_4O_7$-NPs/GCE) setup and an electrochemical cell (10 mL) was used to perform electrochemical experiments. The cyclic voltammetry (CV) technique was employed to study the electron transference mechanism of the modified sensor via 1:1 v/v KCl (0.1 M) and $[Fe(CN)_6]^{3-}$ (0.005 M) as the redox probe. Additionally, the quantitative analysis of APN was performed in triplicates using DPV under optimized conditions (pH 4.0; phosphate buffer; 0.02-sec sampling width; 0.2 sec pulse period; 2-sec quiet time; and 0.05 V amplitude. Before analysis, the solution was purged with nitrogen for 30 min.

Results and discussion

Characterization of $Na_2Fe_4O_7$-NPs

XRD spectroscopy was used to analyze the crystallite nature, size, and % crystallinity of $Na_2Fe_4O_7$-NPs ranging from 20 to 80°. The presence of diffraction peaks at Bragg's diffraction angle (2θ) confirms the hexagonal phase of synthesized $Na_2Fe_4O_7$-NPs with the JCPDS card no. 77–1506 (Fig. 2**a**) [44,45]. The sharpness of indexing peaks in the spectrum suggests the pure crystalline nature of the $Na_2Fe_4O_7$-NPs. In addition, the average size of $Na_2Fe_4O_7$ crystallites was determined via Debye-Scherrer's equation (**Eq. (1)**) [46].

$$D = \frac{Kl}{\beta COS\theta} \tag{1}$$

The symbols D, β, Cos θ, l, and K, represent the crystallite size, peak width at ½ of maximum intensity, diffraction angle, wavelength (1.50 nm), and shape constant (0.94), respectively. The average crystallite size of $Na_2Fe_4O_7$-NPs was determined by applying **Eq. (1)**. The obtained

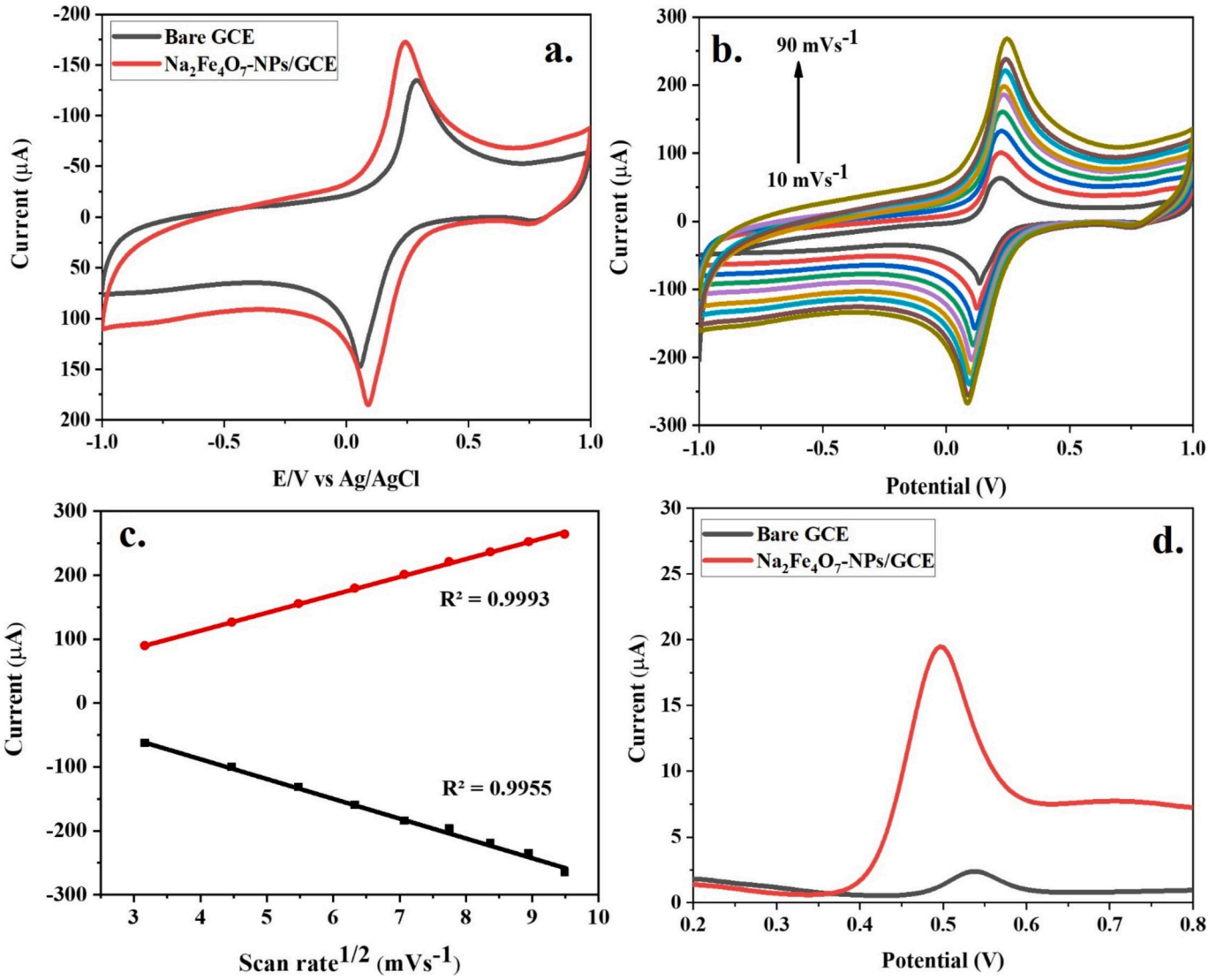

Fig. 4. a. CV response of 5.0 mM $[Fe(CN)_6]^{3-}$ and 0.1 M KCl at bare GCE and $Na_2Fe_4O_7$-NPs/GCE and **b.** at $Na_2Fe_4O_7$-NPs/GCE at different scan rates from 10 – 90 mV s^{-1}**c.** A linear relationship between redox currents and the square root of scan rate and **d.** DPV of bare and $Na_2Fe_4O_7$-NPs/GCE in the 200 μM APN.

average crystallite size of $Na_2Fe_4O_7$-NPs was 7.14 nm, demonstrating its low lattice strain with an increase in structural lattice parameters. These findings are comparable with those reported elsewhere [47]. The crystallinity of the $Na_2Fe_4O_7$-NPs was determined to be 75.8% by following the equation (**Eq. (2)**. The resulting crystallinity showed that a significant portion of the $Na_2Fe_4O_7$-NPs exhibits a well-defined crystalline structure.

$$Crystallinity\ \left(\%\right) = \frac{Area\ of\ crystalline\ peaks}{Total\ Area} \times 100 \qquad (2)$$

FTIR spectroscopy was used for the confirmation of the structure and the chemical functionalities of synthesized $Na_2Fe_4O_7$-NPs [35]. The spectral peaks were found at 3249 and 1638 cm^{-1} due to stretching and bending vibrations of – OH of the water molecule, respectively. These are induced by moisture absorbed by the $Na_2Fe_4O_7$-NPs (Fig. 2**b**) [48]. Moreover, the broadening of the former peak might be attributed to the hydrogen bonding of water molecules. The observed peak at 682 cm^{-1} reflected the Fe–O stretching vibration. The FTIR spectral peak at 871 cm^{-1} is characteristic of hexagonal ferrites which confirmed the successful synthesis of $Na_2Fe_4O_7$-NPs [49].

The UV–visible spectroscopy is widely used to determine the formation of nanoparticles. It measures the absorbance or transmission of light in the visible and ultraviolet regions of the EM (electromagnetic) spectrum by a sample. This spectral analysis was utilized to check the synthesis of $Na_2Fe_4O_7$-NPs in an aqueous media [50]. The absorption band obtained at 298 nm verifies the formation of $Na_2Fe_4O_7$-NPs (Fig. 2**c**). The band gap energy (E_g) of $Na_2Fe_4O_7$-NPs was determined using the Tauc plot. It was found to be 1.475 eV as shown in Fig. 2**d**. The estimated E_g of $Na_2Fe_4O_7$-NPs was also compared with the reported literature such as the E_g values of $MgNb_2O_6$, $Mg_{1-x}Na_xFe_2O_4$, $CoY_xFe_{2-x}O_4$, and Perovskite Bismuth ferrite were 2.76 [51], 2.06 – 2.16 [17], 3.39 – 3.91 [18], and 2.85 eV [19], respectively. This suggested the E_g of synthesized $Na_2Fe_4O_7$-NPs possess comparable and even better optical and electronic properties as compared to the reported studies [52].

The topography and particle size distribution of the sample were studied by the AFM technique [46]. Therefore, AFM was used to study the complementary information about the surface microstructure of prepared ferrites. Fig. 3**a** shows a 3D topographic image of synthesized $Na_2Fe_4O_7$-NPs, indicating semispherical particles with highly rough surfaces. The particle size distribution of $Na_2Fe_4O_7$-NPs ranged between 5.42 and 8.34 nm with an average particle size of 7.09 nm (Fig. 3**b**). It is evident from the AFM that the $Na_2Fe_4O_7$-NPs were uniformly distributed in the nanometer range. Moreover, the resulting narrow range of the distribution of synthesized $Na_2Fe_4O_7$-NPs confirmed their stability.

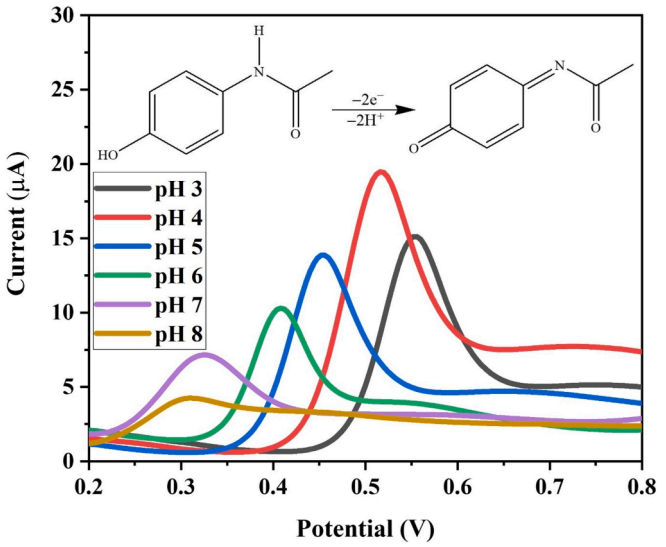

Fig. 5. DPV response of 200 μM APN at different pH (3 – 8) in 0.1 M phosphate buffer showing electrocatalytic oxidation mechanism of APN.

The dynamic light scattering system was used to study the hydrodynamic size distribution of $Na_2Fe_4O_7$-NPs (Fig. 3**c**). The size of $Na_2Fe_4O_7$-NPs was obtained in the range of 1.72 to 37.01 nm with an average size of 20.35 nm. The hydrodynamic size of $Na_2Fe_4O_7$-NPs was greater than the XRD and AFM results, which might be due to the aggregation of nanosized particles in aqueous media.

Zeta potential (electro-kinetic potential) measures surface properties such as stability and charge of the material. Typically, a zeta potential value above ±30 mV (millivolts) indicates good stability, as the electrostatic repulsion between particles prevents their aggregation or flocculation. A high positive or negative zeta potential creates a robust repulsive force that inhibits particle agglomeration and maintains a well-dispersed state. In the current work, the synthesized $Na_2Fe_4O_7$-NPs have an average Zeta potential of −31.2±6.37 mV, indicating the excellent stability of synthesized $Na_2Fe_4O_7$-NPs (Fig. 3**d**).

Electrochemical behaviour of $Na_2Fe_4O_7$-NPs/GCE

CV experimentations were conducted to note the electrochemical features of bare GC electrode and $Na_2Fe_4O_7$-NPs/GCE via a redox probe that involves $[Fe(CN)_6]^{3-}$ (5.0 mM) and KCl (0.1 M) electrolyte at a 50 mVs^{-1} scan rate (Fig. 4**a**). The greater cathodic and anodic peak currents of $Na_2Fe_4O_7$-NPs/GCE as compared to bare GC electrode reveal an increase in surface area-to-volume ratio and outstanding conductive properties of $Na_2Fe_4O_7$-NPs/GCE. The small potential difference in the anodic and cathodic peaks confirmed the uniform transfer of electrons in a redox reaction [53].

The scan rate was also studied ranging from 10 to 90 mVs^{-1} via CV in 1:1 (v/v) mixture of $[Fe(CN)_6]^{3-}$ (10.0 mM) and KCl (0.2 M) as given Fig. 4**b**. A linear relationship was observed between the redox peak currents and scan rate$^{1/2}$ with a strong coefficient of determination ($R^2 > 0.99$) (Fig. 4**c**). The resulting data confirmed that $Na_2Fe_4O_7$-NPs/GCE is electroactive and showed the diffusion-controlled behaviour of electrolyte. Furthermore, the Randles-Sevick Equation (**Eq. (3)**) was used to calculate the electroactive surface area (A) of $Na_2Fe_4O_7$-NPs/GCE.

$$I_p = (2.69 \times 10^5) A D^{1/2} n^{3/2} \upsilon^{1/2} C \quad (3)$$

In **Eq. (3)** the symbols Ip, D, n, υ, and C represent the redox peak current, diffusion coefficient of $[Fe(CN)_6]^{3-}$ (7.6×10^{-6} cm^2/s), electrons number in concerning redox reaction, scan rate (Vs^{-1}) and concentration (mol/cm^3) of the redox probe, respectively [54]. The highly electroactive surface area (A = 0.0822 cm^2) of $Na_2Fe_4O_7$-NPs/GCE demonstrated its outstanding conductive nature for sensing in numerous applications.

Electrocatalytic study of $Na_2Fe_4O_7$-NPs/GCE for APN

The electrocatalytic behaviour of APN (200 μM) was investigated at bare GC electrode and $Na_2Fe_4O_7$-NPs/GCE via DPV in PB (0.1 M) and a prominent oxidation peak of $Na_2Fe_4O_7$-NPs/GCE was observed that confirms the excellent electrocatalytic oxidation properties towards APN when compared to a bare sensor that showed a low oxidation response at 0.548 V (Fig. 4**d**). The $Na_2Fe_4O_7$-NPs like other metal-oxide-based materials possess chemisorbed reactive oxygen species chemically bound to their surfaces that can activate the sensing mechanism by APN interaction and act as a charge transference facilitator for the oxidation of APN via electrocatalysis [55,56]. The electrocatalytic oxidation properties of $Na_2Fe_4O_7$-NPs enable the conversion of APN to acetimidoquinone (Fig. 5) [57].

This innovative role of $Na_2Fe_4O_7$-NPs unlocks new prospects for their application in many other non-opioid analgesic drugs, like APN. Their outstanding current response also confirms their efficient electrocatalytic properties towards the oxidation of APN. Consequently, $Na_2Fe_4O_7$-NPs provide a steady supportive substrate for the manufacture of electrochemical sensors.

Influence of pH and electrolyte

The influence of pH and electrolyte is one of the essential features in electrocatalytic studies. Thus, the electrocatalytic reaction of 200 μM APN was carefully studied across a pH ranging from 3.0 to 8.0 at 50 mVs^{-1} scan rate. The catalytic oxidation of APN was intensely affected by variation in pH (Fig. 5). Hence, pH selection is vital in the electrocatalytic activity of APN at $Na_2Fe_4O_7$-NPs/GCE. The oxidation peak of APN was moved linearly to the lower potential by increasing the pH of the solution from 3.0 to 8.0. However, an excellent oxidation response was obtained at pH 4. Moreover, the narrow band gap of $Na_2Fe_4O_7$-NPs (1.4 eV) may enhance the conductivity and support electron transfer. The proton availability of APN might be greater at pH 4 favoring the interaction of APN with $Na_2Fe_4O_7$-NPs/GCE [58]. The small particle size of $Na_2Fe_4O_7$-NPs might contribute to a larger surface area that leads to better reactivity. This may lead to an increase in the sensing ability of APN [59]. Similarly, *Chipeture et al.* (2019) also reported that pH 4 of the electrolytic solution best suits the electrochemical detection of APN by multiwalled carbon nanotube decorated with bismuth oxide (MWCNT/Bi_2O_3) with a particle size of 21 nm [60].

Furthermore, for optimization of supporting electrolyte the electrocatalytic response of 200 μM APN was studied on the surface of $Na_2Fe_4O_7$-NPs/GCE at pH 4.0 using different electrolyte solutions including acetate buffer, Britton-Robinson buffer, and PB (Fig. 6**a**). The electrocatalytic response of APN was observed in all three electrolyte solutions. However, the maximum amount of APN was detected in PB compared to other electrolytes. Consequently, PB having pH 4.0 was selected as the supporting electrolyte for the later experimentations.

Choice of voltammetric mode

The electrochemical oxidation response of 200 μM APN was also examined using various voltammetric modes such as DPV, LSV (linear sweep voltammetry), and SWV (square wave voltammetry) in PB of pH 4. The oxidation response of APN was observed in all the studied voltammetric modes (Fig. 6**b**). However, DPV provided a prominent oxidation peak for APN compared to SWV and LSV. Therefore, DPV was selected as the best mode for quantitative detection of APN.

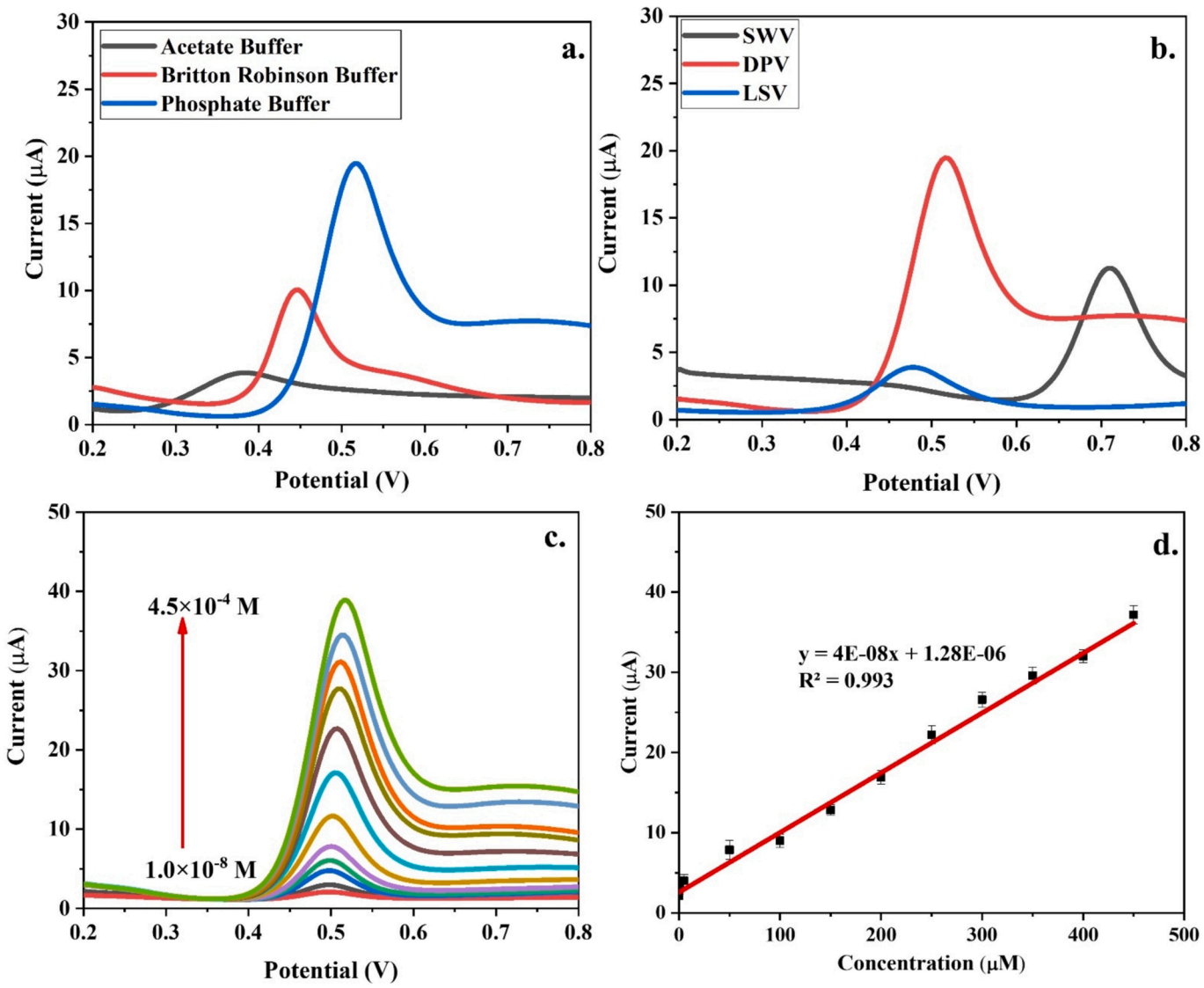

Fig. 6. Differential pulse voltammogram of APN using different **a.** electrolyte solutions, **b.** modes, **c.** Oxidation response of 1.0 x 10^{-8} – 4.5 x 10^{-4} M APN in 0.1 M phosphate buffer and **d.** Linear calibration plot of APN concentration versus current response.

Table 1
Analytical performances of $Na_2Fe_4O_7$-NPs/GCE-based method and other reported studies.

Material	Techniques	Concentration Range (M)	LOD (μM)	RSD (%)	R^2	References
Fe_3O_4-rGO	SWV	$5 \times 10^{-7} - 1 \times 10^{-4}$	0.110	3.03	0.996	[57]
$Ba_{1.14}Cu_{0.82}Fe_{11.65}O_{18.02}$	CV	$1.0 \times 10^{-6} - 1.2 \times 10^{-5}$	0.255	0.255	0.995	[63]
Fe/Fe_3N	DPV	$5.0 \times 10^{-3} - 5.69 \times 10^{-5}$	0.210	3.31	0.994	[64]
VFe_2O_4	DPV	$5.0 \times 10^{-8} - 1.2 \times 10^{-5}$	0.008	<2.0	0.989	[16]
$BaFe_{12}O_{19}$	DPV	$5.0 \times 10^{-6} - 5.0 \times 10^{-4}$	1.5	–-	0.989	[66]
Ni_2P NS	DPV	$5.0 \times 10^{-4} - 4.5 \times 10^{-6}$	0.107	–-	0.997	[4]
Ni/C	DPV	$2.0 \times 10^{-5} - 5.4 \times 10^{-5}$	4.04	4.60	0.996	[65]
$Na_2Fe_4O_7$-NPs	DPV	$1.0 \times 10^{-8} - 4.5 \times 10^{-4}$	0.0027	<3.00	0.992	Present Study

Analytical performance of $Na_2Fe_4O_7$-NPs/GCE for quantitative analysis of APN

DPV provides better resolution comparatively by reducing the impact of background noise [61] when applied to detect APN in PB (0.1 M). Fig. 6**c** shows a remarkable increase in oxidation peak current by increasing the concentration of APN. The resulting data demonstrated that DPV is the most sensitive for accurate APN detection. Hence, a calibration graph was plotted to analyze the electrocatalytic oxidation of APN based on DPV mode. Fig. 6d shows good linearity between the APN concentrations (1.0 x 10^{-8} – 4.5 x 10^{-4} M) and observed currents with the regression equation of I (μA) = 3.72 x 10^{-8}C (μM) + 1.28×10^{-6} (R^2 = 0.993). The limit of detection (LOD) and limit of quantification (LOQ) was calculated to be 2.72 x 10^{-9} and 9.067 x 10^{-9} M by 3σ/slope and 10σ/slope respectively, the symbols σ, 3, and 10 denote the standard deviation of the calibration graph, and the confidence factors respectively [62]. The analytical results of the currently developed voltammetric technique which relies on a modified $Na_2Fe_4O_7$-NPs/GCE for

Table 2
Interference study of numerous species for detection of APN by $Na_2Fe_4O_7$-NPs/GCE.

Interfering species	% Recovery	% RSD
Sucrose	95.15	0.92
Ascorbic acid	96.93	1.73
Levofloxacin	99.02	1.89
Potassium chloride	96.51	1.57
Glucose	97.26	2.04
Hydroquinone	95.78	1.92
Amoxicillin	98.75	1.39
Uric acid	95.93	1.67

Table 3
Application of $Na_2Fe_4O_7$-NPs for voltammetric detection of APN in biological (n = 10), environmental (n = 5), and pharmaceutical samples (n = 9).

Sample	Added (μM)	Found (μM)	Recovery (%)	RSD (%)
Waste-water	–-	0.018	–-	1.94
	10	9.75	97.5	2.03
	50	49.5	99.0	1.57
	100	100.6	100.6	1.79
Urine	–-	BDL	–-	–-
	30	29.0	96.7	0.69
	50	48.1	96.2	1.31
	80	77.8	97.3	1.67
Blood	–-	BDL	–-	–-
	30	28.4	94.7	1.54
	50	52.3	104.6	1.71
	80	79.1	98.9	2.09
Pharmaceutical	**Printed (mg)**	**Found (mg)**	**Recovery (%)**	**RSD (%)**
Tablet1	500	471.6	94.3	1.59
Tablet2	500	459.3	91.9	1.64
Tablet3	500	485.9	97.2	2.13

detecting APN were compared with previous studies. The $Na_2Fe_4O_7$-NPs/GCE-based approach is found to be more sensitive with significantly lower detection limits than reported studies (Table 1) [4,57,63–65]. The synthesis of $Na_2Fe_4O_7$-NPs also contributes to the brilliant electrochemical results obtained by $Na_2Fe_4O_7$-NPs/GCE for APN detection. It improves electron transfer efficiency based on its high catalytic activity and reduces the electron transmission resistance throughout the redox reaction of APN. The achieved outcomes support the consistency of the technique in comparison to reported techniques for APN sensing.

Interference, stability, and repeatability

Various tests were conducted to evaluate the reliability of $Na_2Fe_4O_7$-NPs/GCE to ensure accurate detection, in addition to measuring the target analyte and distinguishing against potential interfering substances [67]. Different interfering substances such as ascorbic acid (AA), sucrose (SU), levofloxacin (LE), potassium chloride (KCl), glucose (GL), hydroquinone (HQ), amoxicillin (AM), and uric acid (UA) were studied with 10 times greater concentration than the analyte (APN) using DPV. Results showed the negligible interference of selected species on $Na_2Fe_4O_7$-NPs /GCE with an RSD of 2.04%, indicating the excellent performance of $Na_2Fe_4O_7$-NPs/GCE for APN sensing in the existence of different sample media (Table 2).

Further, the stability of $Na_2Fe_4O_7$-NPs/GCE was studied by oxidation current responses (n =12) of DPV in 200 μM APN which indicates great similarity (% RSD = 2.11) between the resulting current values and confirms the stable nature of $Na_2Fe_4O_7$-NPs/GCE for electrocatalytic study of APN. Moreover, to assess the stability on different days, the electrode was kept for thirty days, and studies of the 200 μM APN were made on every fifth day. Subsequently, the electrochemical sensor proved acceptable constancy, with approximately ≥ 95% retention rate of peak current. These facts indicate the maintenance of consistency and sustainable sensing over a prolonged period, increasing its repeated use and fitness for longstanding applications. However, the reproducibility of the $Na_2Fe_4O_7$-NPs/GCE fabrication method was inspected as well by developing three $Na_2Fe_4O_7$-NPs/GCE sensors and the oxidation response of 200 μM APN on these three developed $Na_2Fe_4O_7$-NPs/GCE sensors was noted that indicated great similarity (% RSD < 5.0) to each other, enclosing the outstanding reproducibility of currently developed method.

Real sample studies

The concentration of APN was detected in biological samples (human blood and urine), commercially available drugs, and water samples. The reliability of the developed method was examined via the standard addition method for the detection of APN [68]. The results are presented in Table 3 which indicates that the recovery of APN was greater than 90 % in real samples with an RSD of < 3.0 %.

Conclusion

An environmentally friendly sol–gel procedure base synthesis of $Na_2Fe_4O_7$-NPs was done by using *T. indica* fruit extract. The synthesized $Na_2Fe_4O_7$-NPs showed a hexagonal arrangement, porous and rough morphology with a band gap of 1.475 eV and particle size less than 10 nm. A $Na_2Fe_4O_7$-NPs/GCE-based electrochemical sensor was fabricated using the drop-casting method. The proposed sensor possesses practical applicability for the electrochemical sensing of APN using DPV. The $Na_2Fe_4O_7$-NPs/GCE revealed good constancy and repeatability with % RSD < 5.0. The real-world application of the developed technique was evaluated, and the results showed excellent performance, with recovery rates (91.9% – 100.6%) in real samples. The developed $Na_2Fe_4O_7$-NPs/GCE-based electrochemical approach was superior in accuracy, sensitivity, and a broad response range compared to previously published investigations. The proposed economical, eco-friendly, sensitive, and fast electrochemical method using the fabricated sensor is the perfect substitute for the quantitative measurement of APN in numerous sample matrices.

Funding statement

The Researchers Supporting Project Number (RSPD2024R994), King Saud University, Riyadh, Saudi Arabia provided funding for materials characterization and publication for further exploration and discovery. The National Centre of Excellence in Analytical Chemistry (NCEAC), University of Sindh, Jamshoro partially supported the experimental activities of this study.

Approval of ethics

This study was conducted with the informed consent of the selected healthy volunteer participants, who provided biological samples for the electrochemical determination of APN. The selected participants were fully informed of the purpose of the study, utilized procedures, possible risks, and predicted benefits, and were assured of the confidentiality and anonymity of their data. An ethical board is not established for ethical standards-based approval for research involving human subjects. However, the study procedure was designed according to the agreement recommended in the Helsinki Declaration. The proposal for this study was assessed, reviewed and approved by the research and graduate study department, University of Sindh, Jamshoro Pakistan.

CRediT authorship contribution statement

Saima Perveen: Writing – original draft, Methodology, Formal analysis, Data curation. **Jameel Ahmed Baig:** Writing – review & editing, Supervision, Project administration, Conceptualization.

Mohammad Nur-e-Alam: Software, Resources. **Mohsin Kazi:** Software, Resources. **Shahabuddin Memon:** Writing – review & editing, Supervision. **Tasneem Gul Kazi:** Writing – review & editing. **Khalil Akhtar:** Validation, Software, Investigation. **Sajjad Hussain:** Validation, Software, Investigation.

Declaration of competing interest

The authors declare the following financial interests/personal relationships which may be considered as potential competing interests: Mohsin Kazi reports financial support was provided by King Saud University. Jameel Ahmed Baig reports a relationship with University of Sindh that includes: employment. If there are other authors, they declare that they have no known competing financial interests or personal relationships that could have appeared to influence the work reported in this paper.

Acknowledgements

The author would like to extend their sincere appreciation to the Researchers Supporting Project Number (RSPD2024R994), King Saud University, Riyadh, Saudi Arabia.

Data availability

No data was used for the research described in the article.

References

[1] Murugan E, Poongan A, Dhamodharan A. Electrochemical sensing of acetaminophen, phenylephrine hydrochloride and cytosine in drugs and blood serum samples using β-$AgVO_3$/ZrO_2@g-C_3N_4 composite coated GC electrode. J Mol Liq 2022;348:118447.
[2] De Martino, Maurizio, Alberto Chiarugi. Recent advances in pediatric use of oral paracetamol in fever and pain management. Pain Ther 2015;4:149–68.
[3] Wang P, Yuan X, Cui Z, Chunyan Xu, Sun Z, Li J, et al. A nanometer-sized graphite/boron-doped diamond electrochemical sensor for sensitive detection of acetaminophen. ACS Omega 2021;6(9):6326–34.
[4] Shen L, Dong J, Wen B, Wen X, Li J. Facile Synthesis of hollow Fe_3O_4-rGO nanocomposites for the electrochemical detection of acetaminophen. Nanomaterials 2023;13(4):707.
[5] Chaudhary R, Chalotra R, Singh R. Sources and Occurrence of Pharmaceuticals Residue in the Aquatic Environment. In: Pharmaceuticals in Aquatic Environments. CRC Press; 2023. p. 13–29.
[6] Pérez-Ruiz T, Martínez-Lozano C, Tomás V, Galera R. Migration behaviour and separation of acetaminophen and p-aminophenol in capillary zone electrophoresis: analysis of drugs based on acetaminophen. J Pharm Biomed Anal 2005;38(1):87–93.
[7] Khashij M, Mehralian M, Chegini ZG. Degradation of acetaminophen (ACT) by ozone/persulfate oxidation process: experimental and degradation pathways. Pigm Resin Technol 2020;49(5):363–8.
[8] Shaukat A, Hussain K, Bukhari NI, Shehzadi N. Simultaneous determination of paracetamol and lidocaine hydrochloride in detamol injection using RP-HPLC. J Res Pharm 2022;26:609–16.
[9] Caruso TJ, Trivedi S, Chadwick W, Gaskari S, Wang E, Marquez J, et al. A quality improvement project to reduce combination acetaminophen-opioid prescriptions to pediatric orthopedic patients. Pediatric Quality & Safety 2020;5(3):e291.
[10] Lu Z, Guo H, Wei X, Sun L, Pan Z, Liu B, et al. A novel electrochemical sensing platform based on covalent organic frameworks/WC/NH_2-MWCNT for highly selective determination of acetaminophen and 4-aminophenol. Microchem J 2023;193:109075.
[11] Beitollahi H, Tajik S, Aflatoonian MR, Makarem A. Glutathione detection at carbon paste electrode modified with ethyl 2-(4-ferrocenyl-[1, 2, 3] triazol-1-yl) acetate, $ZnFe_2O_4$nano-particles and ionic liquid. J Electrochem Sci Eng 2022;12(1):209–17.
[12] Beitollahi H, Tajik S, Aflatoonian MR, Makarem A. A sensitive Cu (salophen) modified screen-printed electrode for simultaneous determination of dopamine and uric acid. J Electrochem Sci Eng 2022;12(1):199–208.
[13] Jahani M, Peyman HB, Di Bartolomeo A. A voltammetric sensor for the determination of hydroxylamine using a polypyrrole nanotubes-modified electrode. Appl Sci 2022;12(15):7485.
[14] Wang H-B, Hong-Ding Zhang L-L, Gan T, Huang K-J, Liu Y-M. Electrochemical biosensor for simultaneous determination of guanine and adenine based on dopamine-melanin colloidal nanospheres–graphene composites. J Solid State Electrochem 2014;18:2435–42.
[15] Wang J, Yin F, Tang W, Zhang N, Li L, Zheng S, et al. Electrochemical detection of acetaminophen and caffeine using Ag nanoparticles doped metal-organic framework (ZIF-67) composites. Int J Electrochem Sci 2023;18(11):100334.
[16] Hussain S, Sadiq I, Baig JA, Sadiq F, Shahbaz M, Solangi IB, Idrees I, Saeed S, Riaz S, Naseem S. Synthesis and characterization of vanadium ferrites, electrochemical sensing of acetaminophen in biological fluids and pharmaceutical samples. Ceram Int 2023;49(5):8165–71.
[17] Kumar V, Singh RK, Manash A, Das SB, Shah J, Kotnala RK. Structural, optical and electrical behaviour of sodium-substituted magnesium nanoferrite for hydroelectric cell applications. Appl Nanosci 2023;13(6):4573–91.
[18] Das SB, Singh RK, Kumar V, Kumar N, Singh P, Naik NK. Structural, magnetic, optical and ferroelectric properties of Y3+ substituted cobalt ferrite nanomaterials prepared by a cost-effective sol-gel route. Mat Sci Semicon Proc 2022;145:106632.
[19] Sarkar K, Mukherjee S, Mitra MK. Synthesis, characterization and studies on optical, dielectric and magnetic properties of undoped and cobalt doped nanocrystalline bismuth ferrite. J Inst Eng India Ser D 2014;95:135–43.
[20] Boulahouache A, Benlembarek M, Salhi N, Djaballah AM, Rabia C, Trari M. Preparation, characterization and electronic properties of LaFeO3 perovskite as photocatalyst for hydrogen production. Int J Hydrogen Energy 2023;48(39):14650–8.
[21] Shamim A, Charam HA, Nayyab GE, Abid MB. Synthesis, Properties and Applications of Lead Halide Perovskite Nanocrystals. Pak J Anal Environ Chem 2024;25(2).
[22] Shobana MK. Nanoferrites in biosensors–a review. Mater Sci Eng B 2021;272:115344.
[23] Das SB, Singh RK, Kumar V, Murali N, Betal S. Temperature dependent structural, optical, magnetic and dielectric characteristics of cobalt nanoferrites. Bull Mater Sci 2024;47(3):171.
[24] Jadhav VV, Mane RS, Shinde PV, Jadhav VV, Mane RS, Shinde PV. Basics of ferrites: structures and properties. Bismuth-Ferrite-Based Electrochemical Supercapacitors 2020:37–45.
[25] Dippong T, Levei EA, Cadar O. Investigation of structural, morphological and magnetic properties of MFe_2O_4 (M= Co, Ni, Zn, Cu, Mn) obtained by thermal decomposition. Int J Mol Sci 2022;23(15):8483.
[26] Vidya YS, Manjunatha HC, Sridhar KN, Seenappa L, Munirathnam R, Chinnappareddy B. Brief review on magnetic properties of nanoferrites. Inorg Chem Commun 2023:111408.
[27] El-Shater RE, El Shimy H, Saafan SA, Darwish MA, Zhou DI, Trukhanov AV, Trukhanov SV, Fakhry F. Synthesis, characterization, and magnetic properties of Mn nanoferrites. J Alloy Compd 2022;928:166954.
[28] Srinivasan SY, Paknikar KM, Bodas D, Gajbhiye V. Applications of cobalt ferrite nanoparticles in biomedical nanotechnology. Nanomedicine 2018;13(10):1221–38.
[29] Cuong HN, Pansambal S, Ghotekar S, Oza R, Hai NTT, Viet NM, Nguyen VH. New frontiers in the plant extract mediated biosynthesis of copper oxide (CuO) nanoparticles and their potential applications: A review. Environ Res 2022;203:111858.
[30] Akhtar K, Baig JA, Solangi SA, Perveen S, Hussain S, Kazi TG, Afridi HI, Abbasi F. Phytoextract based synthesis of TiO_2. Al_2O_3 nanocomposites for efficient electrocatalytic detection of acetaminophen from environmental and pharmaceutical samples. Ceram Int 2024;50(7):11012–21.
[31] Tamboli QY, Patange SM, Mohanta YK, Sharma R, Zakde KR. Green synthesis of cobalt ferrite nanoparticles: An emerging material for environmental and biomedical applications. J Nanomater 2023;2023(1):9770212.
[32] Giordano C, Antonietti M. Synthesis of crystalline metal nitride and metal carbide nanostructures by sol–gel chemistry. Nano Today 2011;6(4):366–80.
[33] Perveen S, Hol A, Baig JA, Sherazi STH, Akhtar K, Hussain S, Abbasi F. Sodium nanoferrite-based solid phase extraction: a green method for the simultaneous determination of cadmium, copper, and lead. J Anal Atom Spectrom 2024;39(11):2884–92.
[34] Bhanbhro P, Baig JA, Solangi IB, Kazi TG, Akhtar K, Nadeem A, Perveen S, Abbasi F, Hussain S. Solangi, S.A.Cadmium oxide/calcium ferrite nanocomposite-based enhanced electrochemical sensing of metronidazole. Microchem J 2024;207:111820.
[35] Hussain S, Sadiq I, Khan HM, Idrees M, Sadiq F, Shah A, et al. Characterization and curve fittings of Mg^{+2} substituted R-type hexagonal ferrites. Phys B Condens Matter 2021;605:412642.
[36] Kumar V, Singh RK, Sarkar K, Kumari R, Shah J, Kotnala RK. A Novel Ag-$MgFe_2O_4$ nanocomposite based Hydroelectric Cell: Green energy source illuminating the future. J Alloy Compd 2024:175032.
[37] Kumar V, Kumar N, Das SB, Singh RK, Sarkar K, Kumar M. Sol-gel assisted synthesis and tuning of structural, photoluminescence, magnetic and multiferroic properties by annealing temperature in nanostructured zinc ferrite. Mater Today Proc 2021;47:6242–8.
[38] Sarkar K, Harsh H, Rahman Z, Kumar V. Enhancing the structural, optical, magnetic and ferroelectric properties of perovskite $BiFeO_3$ through metal substitution. Chem Phys Impact 2024;8:100478.
[39] Hussain S, Sadiq I, Baig JA, Bertotti M, Riaz S. An R-type hexagonal ferrite nanoparticles-based electrochemical sensor for Levofloxacin detection in pharmaceutical and clinical specimens. Microchem J 2024;201:110690.
[40] Tangra AK, Lotey GS. Synthesis and investigation of structural, optical, magnetic, and biocompatibility properties of nanoferrites $AFeO_2$. Curr Appl Phys 2021;27:103–16.
[41] Solunke A, Barote VK, Sonawane B, Shirsath SE, Kadam RH, Shinde VS. Sol-gel synthesis of Fe-rich cobalt ferrite nanoparticles and influence of pH concentration. Mater Today Proc 2023;92:1225–30.
[42] Yilmaz S, Bas Z, Sadikoglu M, Yagmur S, Saglikoglu G. Sensitive voltammetric determination of paracetamol on poly (4-Aminobenzene Sulfonic Acid) modified glassy carbon electrode. Int J Electrochem Sci 2016;11(7):6244–55.

[43] Yuan D, Yuan X, Zhou S, Zou W, Zhou T. N-Doped carbon nanorods as ultrasensitive electrochemical sensors for the determination of dopamine. RSC Adv 2012;2(21):8157–63.
[44] Zhang X, Geng Z, Jian J, He Y, Lv Z, Liu X, et al. Potassium ferrite as heterogeneous photo-fenton catalyst for highly efficient dye degradation. Catalysts 2020;10(3):293.
[45] Zhang H, Li Y, Wang W, Ma L, Chen L. In: A Study on Aggressiveness of KCl to Steel Material in High Temperature in Biomass Boilers. Atlantis Press; 2015. p. 164–7.
[46] Akhtar K, Baig JA, Kazi TG, Afridi HI, Talpur FN, Solangi IB, Samaijo S. Novel fluoride selective voltammetric sensing method by amino phenylboronic acid-zirconium oxide nanoparticles modified gold electrode. Microchem J 2022;174:107073.
[47] Kumar D, Singh M, Singh AK. Crystallite size effect on lattice strain and crystal structure of Ba1/4Sr3/4MnO3 layered perovskite manganite. In AIP Conference. Proceedings 2018;(1953):1.
[48] Elahi A, Ahmad M, Ali I, Rana MU. Preparation and properties of sol–gel synthesized Mg-substituted Ni2Y hexagonal ferrites. Ceram Int 2013;39(2):983–90.
[49] Ohlan A, Singh K, Chandra A, Dhawan SK. Microwave absorption behavior of core– shell structured poly (3, 4-ethylenedioxy thiophene)–barium ferrite nanocomposites. ACS Appl Mater Interfaces 2010;2(3):927–33.
[50] Titus D, Samuel EJJ, Roopan SM. Nanoparticle characterization techniques. In: Green Synthesis, Characterization and Applications of Nanoparticles. Elsevier; 2019. p. 303–19.
[51] Sarkar K, Kumar V. Luminescence and dielectric investigations of crystalline niobate nanoceramics prepared through aqueous chemical process. Phys Scr 2024;99(10):105992.
[52] Wang Y, Huang C, Li D, Huang F, Zhang X, Huang K, et al. Stress-and electric-field-induced band gap tuning in hexagonal boron phosphide layers. J Phys Condens Matter 2019;31(46):465502.
[53] Kannan PK, Moshkalev SA, Rout CS. Electrochemical sensing of hydrazine using multilayer graphene nanobelts. RSC Adv 2016;6(14):11329–34.
[54] Meenakshi S, Jancy Sophia S, Pandian K. High surface graphene nanoflakes as sensitive sensing platform for simultaneous electrochemical detection of metronidazole and chloramphenicol. Mater Sci Eng C 2018;90:407–19.
[55] Montazeri A, Jamali-Sheini F. Enhanced ethanol gas-sensing performance of Pb-doped In_2O_3 nanostructures prepared by sonochemical method. Sens Actuators B 2017;242:778–91.
[56] Khosravi-Hamoleh A, Abrishamkar M, Cheraghizade M. Simultaneous electrochemical sensing of ceftriaxone and piroxicam using zeolite modified electrode for medical applications. Electroanalysis 2021;33(8):1866–70.
[57] Wei M, Wenbo Lu, Liu G, Jiang Y, Liu X, Bai L, et al. Ni2P nanosheets: A high catalytic activity platform for electrochemical detection of acetaminophen. Chin J Chem 2021;39(7):1849–54.
[58] Phogat P, Jha R, Singh S. Electrochemical analysis of thermally treated two dimensional zinc sulphide hexagonal nano-sheets with reduced band gap. Phys Scr 2023;98(12):125962.
[59] Zhao Y, Gao J, Liu C, Chen X, Zhenhai Xu. The particle-size effect of waste clay brick powder on its pozzolanic activity and properties of blended cement. J Clean Prod 2020;242:118521.
[60] Chipeture AT, Apath D, Moyo M, Shumba M. Multiwalled carbon nanotubes decorated with bismuth (III) oxide for electrochemical detection of an antipyretic and analgesic drug paracetamol in biological samples. J Anal Sci Technol 2019;10:1–13.
[61] Abass MH, Hassan ZK, Al-Jabary KMA. "Assessment of heavy metals pollution in soil and date palm (Phoenix dactylifera L.) leaves sampled from Basra/Iraq governorate." Advances. Environ Sci 2015;7(1):52–9.
[62] Hussain S, Sadiq I, Baig JA, Sadiq F, Solangi IB, Akhtar K, Solangi SA, Idress M, Riaz S, Naseem S. Electrocatalytic sensing of metronidazole by R-type hexagonal nanoferrites modified electrode. Inorg Chem Commun 2023;153:110832.
[63] Granja-Banguera CP, Silgado-Cortázar DG, Morales-Morales JA. Transition metal substituted barium hexaferrite-modified electrode: Application as electrochemical sensor of acetaminophen. Molecules 2022;27(5):1550.
[64] Guo L, Hao L, Zhang Y, Yang X, Wang Q, Wang Z, et al. Metal-organic framework precursors derived Ni-doping porous carbon spheres for sensitive electrochemical detection of acetaminophen. Talanta 2021;228:122228.
[65] Pierpaoli M, Jakóbczyk P, Dec B, Giosue C, Czerwińska N, Lewkowicz A, Ruello ML, Bogdanowicz R. A novel hierarchically-porous diamondized polyacrylonitrile sponge-like electrodes for acetaminophen electrochemical detection. Electrochim Acta 2022;430:141083.
[66] Abbasi F, Solangi IB, Baig JA, Hussain S, Perveen S, Akhtar K, Solangi SA, Bhanbhro P. Innovative approach for trace level detection of mefenamic acid by ferrite nanocomposite-based electrochemical sensor. Mater Today Commun 2024;40:109739.
[67] Xie X, Wang DP, Guo C, Liu Y, Rao Q, Lou F, Li Q, Dong Y, Li Q, Yang HB, Hu FX. Single-atom ruthenium biomimetic enzyme for simultaneous electrochemical detection of dopamine and uric acid. Anal Chem 2021;93(11):4916–23.
[68] Baig JA, Muhammad M, Akhtar K, Afridi HI, Kazi TG, Mirza J, Solangi SA, Bhutto AA. Selective electrochemical sensing of cefixime by silver nanoparticle amalgam paste microelectrode. J Mater Sci: Mater Electron 2022;33(17):13926–38.